JOURNAL OF AIRCRAFT
Vol. 45, No. 2, March–April 2008

Reduced-Size Aeroservoelastic Modeling and Limit-Cycle-Oscillation Simulations with Structurally Nonlinear Actuators

P. Gold* and M. Karpel†
Technion–Israel Institute of Technology, 32000 Haifa, Israel

DOI: 10.2514/1.28933

Reduced-size aeroservoelastic equations of motion are constructed and used for stability analysis and maneuver simulations with control-surface actuator nonlinearity caused by free play. A linear modal-based state-space aeroservoelastic formulation is expanded to address the nonlinear actuator stiffness characteristics by means of nonlinear feedback loops. The fictitious-mass method is used to accurately account for the actuator stiffness changes during simulations. The direct-force modeling approach is found to be more suitable for representing the stiffness-actuation mechanics than the control-mode approach. A modal-based aeroelastic trim analysis algorithm that takes into account the actuator free play is used to determine the initial aeroelastic states of the aircraft in a steady flight. Symmetric and antisymmetric normal modes of an unmanned aerial vehicle model with disconnected actuators are combined for asymmetric aeroservoelastic time-domain equations of motion with nonlinear actuator effects and full control-system dynamics. Simulations of the complete aircraft structural dynamic response to maneuver commands exhibit asymmetric limit-cycle oscillations when one of the actuator forces changes sign.

I. Introduction

AEROSERVOELASTICITY (ASE) deals with the interaction of the aeroelastic and control systems. Many modern control design techniques and simulations with nonlinear effects require the aeroservoelastic equations of motion to be cast in a first-order time-domain (state-space) form. The structure is commonly represented in these equations by its normal modes that serve as generalized coordinates. The unsteady generalized aerodynamic force coefficient matrices are approximated by rational functions in the complex Laplace domain [1,2]. The resulting state-space equations can be easily augmented by standard control-system models to provide ASE constant-coefficient equations, for which ASE stability and response analyses can be carried out using commercial software tools such as MATLAB and ZAERO [3].

The research on nonlinear aeroelasticity has received much attention in the last decade. A description of the work on free-play nonlinearities, including a literature overview, may be found in [4], focusing on correlations between theory and experiment. There have been many recent studies concerning limit-cycle oscillations (LCO) due to free play. An excellent review of these studies may be found in [5]. According to [5], there have been many cases of aircraft experiencing flutter-induced LCO as a result of control-surface free play. These events are not well documented in the public literature, but they are well known and accepted among practitioners. One of the recent references regarding the flutter/LCO caused by control-surface free play in Airbus aircraft may be found in [6].

An important source of nonlinearity that often leads to LCO is mechanical free play in control-surface-actuator mechanisms. Numerical integration techniques of state-space models for aeroelastic systems with free play are discussed in [7]. The time-domain models allow the description of the nonlinear behavior in an exact manner. However, the need to approximate the unsteady aerodynamics by rational function approximation may complicate the process and involve some loss of accuracy. Hence, many investigations (such as that of [8]) resort to frequency-domain equations, with the nonlinearity represented by describing functions. In both time and frequency domains, the introduction of nonlinear structural elements into the ASE system is not a simple matter, because the parametric changes affect the normal modes on which the equations of motion are based. A common approach for dealing with changing structural parameters is by assuming that the structural displacement vectors over the entire range of structural changes can be expressed as linear combinations of a single set of modes. However, this assumption might be grossly inaccurate in cases of large local structural changes to complicated finite element models. Reference [4] suggests repeating the finite element analysis in such cases, which might be inefficient and inaccurate, due to the change of coordinates during time simulations.

The fictitious-mass (FM) approach [9] was used in several applications (such as in [10]) to allow large structural variations without changing the modal basis in cases in which a small number of elements are affected by nonlinearities. With the FM approach, the degrees of freedom to which the affected elements are connected are loaded with fictitious masses when the normal modes are generated. This causes the low-frequency modes to contain the necessary local deformations to adequately account for the structural changes in time-domain simulations. This approach was expanded for ASE systems with piezoelectric actuators [11] by using stiffness-proportional fictitious-mass matrices that lead to lower-order models. It was also used for calculating eigenvalue sensitivities to actuator stiffness parameters [12].

The purpose of the work described in this paper is to expand the state-space ASE formulation for the construction of efficient ASE equations of motion in which the control-surface actuators are grossly nonlinear, such as in the case of actuator free play. Fictitious masses are used to facilitate the use of a single set of modes as fixed generalized coordinates. Various techniques for the representation of the control forces are investigated and a preferred technique is chosen. Symmetric and antisymmetric normal modes are used for complete aircraft simulations with the nonlinear effects causing structural coupling between them. The numerical example is of a control-augmented uninhabited aerial vehicle (UAV) flying at sea level between 10 and 40 m/s. The ZAERO aerodynamic panel is shown in Fig. 1. Roll maneuvers are simulated with actuator free play

Presented as Paper 1936 at the 47th AIAA/ASME/ASCE/AHS/ASC Structures, Structural Dynamics, and Materials Conference, Newport, RI, 1–4 May 2006; received 1 December 2006; revision received 11 November 2007; accepted for publication 11 November 2007.

*Graduate Student, Faculty of Aerospace Engineering.
†Professor, Sanford Kaplan Chair in Aerospace Engineering, Faculty of Aerospace Engineering. Associate Fellow AIAA.

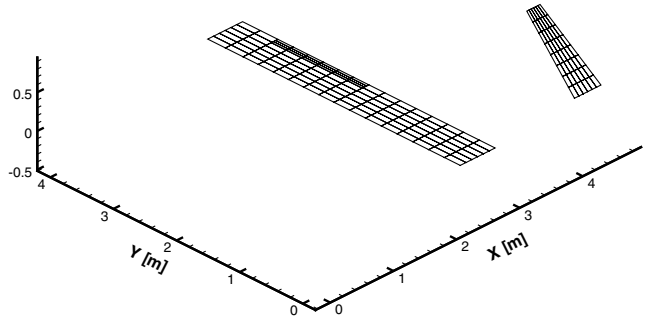

Fig. 1 UAV aerodynamic model.

in both ailerons. The simulations start from a trimmed 1-g level flight solution that takes into account the actuator free play.

II. Structural Model with Fictitious Masses

A standard air vehicle finite element model is used as a numerical example, with fictitious masses added to the aileron actuator model. The MSC.Nastran structural model is shown in Fig. 2. The aileron actuator has a dynamic part for which the output is the commanded rotation δ_c about the hinge line relative to the wing, and it has a rotational spring that connects this output to the aileron structure. The actual aileron displacement is $\delta_a = \delta_c + \delta_s$, where δ_s is the rotational deformation of the spring. The dynamic part is ignored in the structural model, with $\delta_c = 0$, such that the spring connects the aileron directly to the wing. With no free play, the stiffness of the rotational spring is $k_\theta = 30$ Nm/rad. To successfully model the nonlinear behavior, it is vital to properly account for the nonlinear effects during time simulations. In our case, we represent the mechanical free play of the aileron actuator by changing the actuator stiffness from its nominal value to zero during the simulations, while the aileron angle is in the free-play zone. To avoid numerical difficulties in the simulation process, the zero stiffness is represented by $k_\theta = 0.001$ Nm/rad.

A standard modal approach might not account properly for the structural deformations at and near locations of large stiffness changes. The FM method [9–11] can be used to improve the representation of selected local deformations in the set of low-frequency modes taken into account. The normal modes are calculated with selected degrees of freedom loaded by large fictitious masses. Their inertial effects are later removed, leaving the modal basis with a high-frequency subset of local-deformation modes to be included in the subsequent modal-based analysis. Normal modes analysis is performed by solving the eigenvalues problem:

$$[K_{aa}][\phi_{ai}] = [M_{aa} + M_F][\phi_{ai}][\Omega_i] \tag{1}$$

where $[K_{aa}]$ and $[M_{aa}]$ are the full discrete-coordinate mass and stiffness matrices after the application of displacement constraints, $[\phi_{ai}]$ is the associated low-frequency normal modes for subsequent analyses, $[\Omega_i]$ is a diagonal matrix with the respective eigenvalues, and $[M_F]$ is the matrix of the added fictitious masses at desired locations. Equation (1) can be solved by standard eigenproblem codes for $[\phi_{ai}]$ and $[\Omega_i]$. With relatively large fictitious masses, $[\phi_{ai}]$ contains significant local deformation at the vicinity of these masses, which implies high-fidelity representation of these locations in the modal basis. These eigenvalues and eigenvectors are, of course, substantially different from those of the actual structure. However, by assuming that the actual normal modes $[\phi_{ah}]$ are linear combinations of $[\phi_{ai}]$, we can resort to the actual model by first removing the effect of $[M_F]$ from the generalized mass matrix:

$$[\tilde{M}_{ii}] = [M_{ii}] - [\phi_{ai}]^T[M_F][\phi_{ai}] \tag{2}$$

where $[M_{ii}]$ is the diagonal generalized mass matrix associated with $[\phi_{ai}]$. In addition, the stiffness properties of the model can be changed by introducing a differential stiffness matrix $[\Delta K]$ that modifies the generalized stiffness matrix:

$$[\tilde{K}_{ii}] = [K_{ii}] + [\phi_{ai}]^T[\Delta K][\phi_{ai}] \tag{3}$$

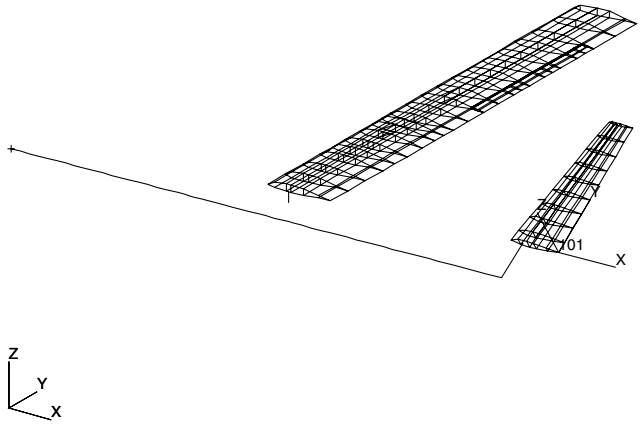

Fig. 2 UAV structural model.

The premultiplication of Eq. (1) by $[\phi_{ai}]^T$ and the replacement of the resulting $[M_{ii}]$ and $[K_{ii}]$ by $[\tilde{M}_{ii}]$ and $[\tilde{K}_{ii}]$ form the eigenproblem:

$$[\tilde{K}_{ii}][\psi] = [\tilde{M}_{ii}][\psi][\Omega_h] \tag{4}$$

which, being of low order, can be easily solved for all of its eigenvalues $[\Omega_h]$ and eigenvectors $[\psi]$. The mode shapes after removing the fictitious masses become

$$[\phi_{ah}] = [\phi_{ai}][\psi] \tag{5}$$

The low eigenvalues in $[\Omega_h]$ and the associated modes in $[\phi_{ah}]$ are typically almost identical to those of the respective finite element models. The highest-frequency modes reflect local deformations and are not necessarily actual physical natural modes. They are included, however, to account for the local deformations in subsequent analyses. The number of these local-deformation modes is up to the rank of $[M_F]$, depending on the number of modes taken into account and the size of the fictitious-mass terms.

In our numerical example, the use of a single fictitious mass at the δ_s degree of freedom provides a convenient way for an adequate evaluation of the actuator behavior while the aileron travels in and out the free-play zone. To demonstrate, a set of 17 symmetric normal modes up to 60 Hz was generated using MSC.Nastran, with δ_s assigned with the soft stiffness actuator $k_q = 0.001$ Nm/rad and loaded with a large fictitious moment of inertia $m_f = 100$ kg m^2. The frequencies and mode shapes were then corrected for those of the cleaned model by solving Eq. (4) with the fictitious inertia removed and the stiffness properties unchanged. Another set of normal modes was then calculated for the case of the stiff (nominal) actuator with the generalized stiffness modified, with $[\Delta K]$ having one nonzero term: $k_q = 30$ Nm/rad. The natural frequencies of the baseline FM model are compared in Table 1 with those obtained after the inertia cleaning process, with and without the stiffness change. The cleaned frequencies are also compared with those obtained from NASTRAN by direct, separate, normal mode analyses. It can be observed that even though the cleaning process started in both cases with the same set of FM modes, the results are practically identical to those obtained directly in separate runs, except for the last frequency in each. This frequency is not a natural frequency, but a synthetic one that represents local deformations associated with the spring and the surrounding structure.

The use of a single set of FM modes accurately yields the almost-zero natural frequency of aileron rotation in the low-stiffness case of Table 1 (0.06 Hz) and its nominal frequency in the high-stiffness case (8.238 Hz). The computation process also correctly valuates the effects of the aileron frequency increase on all the other frequencies: namely, slightly reducing the wing natural frequency (3.577 Hz), due to switch with the aileron frequency, and keeping the other natural frequencies almost unchanged. The high accuracy demonstrated in Table 1 by comparisons with direct NASTRAN solutions proves that the use of FM modal coordinates provides an accurate treatment of the actuator nonlinearity in modal-based analyses with large actuator stiffness changes.

Table 1 Symmetric natural frequencies of the FM, zero-stiffness, and nominal-stiffness models

		$k_\theta = 0.001$ Nm/rad		$k_\theta = 30$ Nm/rad	
Mode	Nastran FM included, Hz	FM cleaned, Hz	Direct Nastran analysis, Hz	FM cleaned, Hz	Direct Nastran analysis, Hz
1	0	0	0	0	0
2	0	0	0	0	0
3	0	0	0	0	0
4	0.001	0.060	0.060	3.577	3.577
5	3.606	3.817	3.817	8.328	8.329
6	9.709	9.809	9.809	9.914	9.915
7	12.450	15.640	15.641	15.754	15.754
8	16.064	22.703	22.703	22.731	22.731
9	22.735	22.871	22.871	23.504	23.503
10	24.523	33.709	33.645	35.618	35.577
11	36.911	37.064	37.061	37.172	37.165
12	39.907	43.393	43.386	43.451	43.445
13	43.712	49.584	49.584	49.584	49.584
14	49.584	51.792	51.791	51.793	51.792
15	51.794	56.647	56.560	56.679	56.654
16	56.730	58.800	58.430	58.827	58.766
17	58.869	84.073	59.247	100.288	60.005

III. Open-Loop Aeroelastic Equations of Motion

The modal-based equations of motion of aeroelastic systems excited by control-surface-actuator displacements are commonly based on the control-mode approach [1,2] that considers the aerodynamic and inertial forces due to control-surface motion explicitly. A control mode is defined by the static displacements of the unloaded structure due to a unit actuator output, typically defined in terms of the control-surface rotation angle. This approach is problematic when the actuator is disconnected from the structure, such as when the control surface passes through a free-play zone. Hence, an alternative direct-force approach was taken in this work.

The direct-force approach [11] is based on the direct application of the actuation forces to the structure, whereas the aerodynamic and inertial control-surface effects are part of the structural response. Its main disadvantage is that it requires high-accuracy representation of the structural displacements at the points to which the forces are applied. This problem is overcome by using fictitious masses, as discussed previously. Another advantage of the direct-force approach in our work is that it allows the structure to be represented by a linear model, whereas the nonlinear actuator is represented by a nonlinear feedback loop. The state-space time-domain aeroelastic equation of motion in modal coordinates, subjected to direct-force excitation, reads

$$\{\dot{x}_{ae}\} = [A_{ae}]\{x_{ae}\} + [B_{ae}]\{M_{\text{inp}}\} \tag{6}$$

where

$$\{x_{ae}\} = \begin{Bmatrix} \xi \\ \dot{\xi} \\ x_a \end{Bmatrix}, [A_{ae}]$$

$$= \begin{bmatrix} 0 & I & 0 \\ -[\bar{M}]^{-1}[K_{hh} + qA_0] & -[\bar{M}]^{-1}\left[B_{hh} + \frac{qL}{V}A_1\right] & -q[\bar{M}]^{-1}[D] \\ 0 & [E] & \frac{V}{L}[R] \end{bmatrix},$$

$$[B_{ae}] = \begin{bmatrix} 0 \\ \bar{M}^{-1}[\phi_{sh}]^T \\ 0 \end{bmatrix}, \qquad [\bar{M}] = [M_{hh}] + \frac{qL^2}{V^2}[A_2]$$

where $\{\xi\}$ is the vector of modal displacements; $\{x_a\}$ is an augmenting vector of aerodynamic lag states; $\{M_{\text{inp}}\}$ is the vector of moments about the control-surface hinge lines applied by the actuators; q is the dynamic pressure; L is a reference length; V is the true air velocity; $[M_{hh}]$, $[K_{hh}]$, and $[B_{hh}]$ are the generalized mass, stiffness, and damping matrices associated with $[f_{ah}]$ of Eq. (5); and $[f_{sh}]$ is the row partition of $[f_{ah}]$ associated with $\{M_{\text{inp}}\}$. The remaining matrices in Eq. (6) are of the aerodynamic rational function approximation:

$$[\tilde{Q}_h(ik)] = [A_0] + [A_1]ik + [A_2](ik)^2 + [D](ik[I] - [R])^{-1}[E]ik \tag{7}$$

where $k = \omega L/V$ and the coefficient matrices are found by either Roger's or the minimum-state approximation procedures that fit the data matrices along the imaginary axis of the Laplace domain $i\omega$ by using the least-squares approach [1,2].

The nonlinearity in this work is due to actuator free play when the aileron hinge moments change sign. The hinge moment of each aileron, $-M_{\text{inp}}$, vs the rotation angle at the actuation point relative to the displacement command δ_s is shown in Fig. 3. For the sake of simplicity, the free-play zone $\pm\delta_f$ is assumed to be symmetric about $\delta_s = 0$.

The direct-force terms on the right side of Eq. (6) facilitates the introduction of feedback forces based on the elastic dynamic response $\{\delta_s(t)\}$ of the ailerons:

$$\{\delta_s(t)\} = \{\delta_a(t)\} - \{\delta_c(t)\} \tag{8}$$

where $\{\delta_c(t)\}$ is the vector of actuator outputs and $\{\delta_a(t)\}$ is the vector of actual aileron deflections:

$$\{\delta_a(t)\} = [\phi_{sh}]\{\xi(t)\}$$

Symmetric and antisymmetric structural modes can be extracted from a half-model with symmetric and antisymmetric boundary conditions. In our case, the modes were generated with the fictitious masses of the previous section and without including the actuator stiffness using the right-side model of Fig. 2. Because this modal basis has already been shown to yield accurate dynamic properties

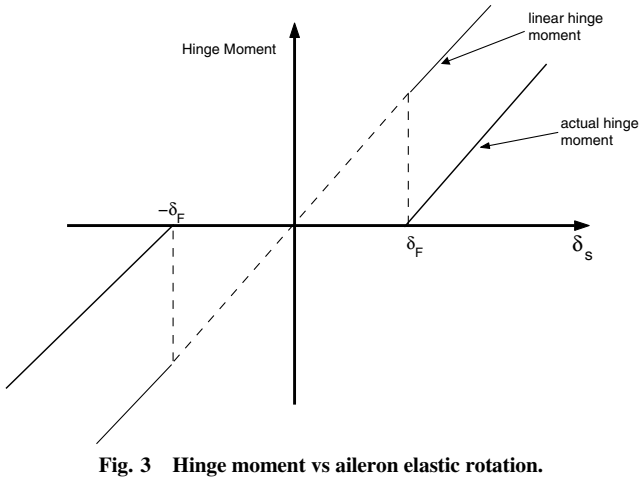

Fig. 3 Hinge moment vs aileron elastic rotation.

for both the nominal k_θ and for the zero-stiffness case, the state-space model is adequate over the entire range of the nonlinear stiffness changes. The model of Eq. (6) includes both symmetric and antisymmetric modes to allow asymmetric response when only one actuator enters the free-play zone. Because any shape of a geometrically symmetric structure such as ours can be represented as a superposition of symmetric and antisymmetric functions, and because the symmetric and antisymmetric modes provide adequate bases in the respective separate analyses, it may be assumed that the assembly of the two types of modes adequately represents the asymmetric motion. For the case of two control surfaces, right and left ailerons, Eq. (8) becomes

$$\begin{Bmatrix} \delta_{s_r} \\ \delta_{s_l} \end{Bmatrix} = \begin{bmatrix} \phi_{sh_s} & \phi_{sh_a} \\ \phi_{sh_s} & -\phi_{sh_a} \end{bmatrix} \begin{Bmatrix} \xi_s \\ \xi_a \end{Bmatrix} - \begin{Bmatrix} \delta_{c_r} \\ \delta_{c_l} \end{Bmatrix} \tag{9}$$

where the new subscripts r and l relate to the right and left ailerons, and s and a relate to the symmetric and antisymmetric modes. The symmetric and antisymmetric generalized structural and aerodynamic properties are obtained separately and appear in $[A_{ae}]$ of Eq. (6) with no coupling terms. The modal matrix $[f_{sh}]$ in $[B_{ae}]$ is that of Eq. (9). The input moments in Eq. (6) relate to the right- and left-aileron deflections by the nonlinear relation:

$$M_r = \begin{cases} -k_\theta(\delta_{s_r} + \delta_{f_r})/2 & @\delta_{s_r} < -\delta_{f_r} \\ 0 & @ -\delta_{f_r} \le \delta_{s_r} \le \delta_{f_r} \\ -k_\theta(\delta_{s_r} - \delta_{f_r})/2 & @\delta_{s_r} > \delta_{f_r} \end{cases} \tag{10}$$

and M_l is similarly determined from the deflection parameters of the left aileron. The division by 2 is because the generalized matrices are based on half-models. It was assumed in this section that when the structure is unloaded and there are no control commands, the ailerons are located in the middle of the free-play zone with $\{\delta_s\} = \{0\}$.

It can be observed in Eq. (10) that when $\{\delta_f\} = \{0\}$, the system is linear with the nominal actuator stiffness, and when $\{\delta_f\}$ is large, the system is linear with zero actuator stiffness. The substitution of Eqs. (9) and (10) with $\{\delta_c\} = \{0\}$ into Eq. (6) yields the linear system matrix for which the roots indicate linear flutter. Root-loci stability analyses, one with the actuators disconnected and one with the actuators connected with no free play, were performed at sea level with incompressible aerodynamics. Only one flutter case was obtained within the flight envelope: a symmetric aileron flutter at $V_f = 10.7$ m/s and $\omega_f = 3.16$ Hz, near the first wing-bending frequency.

IV. Closed-Loop-Maneuver Equations of Motion

A maneuver simulation should start from a steady trimmed flight to determine the initial aileron deflections relative to the free-play zone. The ZAERO code was used to perform symmetric modal-based trim analysis at 1-g level flight at 25-m/s sea level, with the actuator at its nominal value k_θ. The longitudinal trim was performed with the stabilizer. Because the elastic rotation of the aileron actuator was expected to be negative, the trim analysis was performed with a fixed commanded symmetric deflection of the aileron of $\delta_f = -0.5$ deg. The trimmed solution indicated negative elastic rotation of the aileron of $\delta_{\text{ail}} = -0.5$ deg, which was added to the commanded δ_f to obtain the symmetric aileron position of $\delta_t = -1.0$ deg at 1-g level flight. For the sake of simplicity, it was assumed here that the right- and left-actuator free-play values are the same.

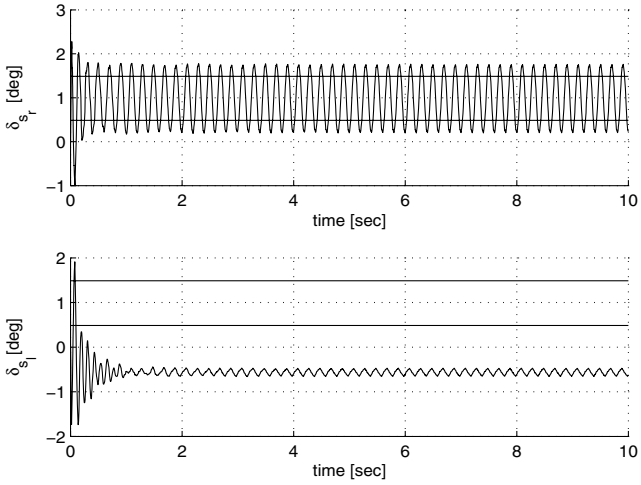

Fig. 4 Open-loop LCO simulation in response to a sudden change in the aileron command.

The aircraft maneuvers described next are relative to the trimmed 1-g solution: namely, they start from zero deformations and input moments. The equations of motion of the previous section should be used in this case, with the input moments of Eq. (10) shifted by $k_\theta(\delta_t + \delta_f)/2$ and with δ_s shifted by δ_t. The resulting input moments become

$$M_r = \begin{cases} -k_\theta \delta_{s_r}/2 & @\delta_{s_r} < -\delta_t - \delta_f \\ k_\theta(\delta_t - \delta_f)/2 & @ -\delta_t - \delta_f \le \delta_{s_r} \le -\delta_t + \delta_f \\ -k_\theta(\delta_{s_r} - 2\delta_f)/2 & @\delta_{s_r} > -\delta_t + \delta_f \end{cases} \tag{11}$$

and M_l is similarly determined from the deflection parameters of the left aileron. The output Eq. (9) remains unchanged. The number of states in the plant Eq. (6) for the maneuver simulations is

$$n_p = 2(n_{h_s} + n_{h_a}) + n_{a_s} + n_{a_a} \tag{12}$$

where n_{h_s} and n_{h_a} are the number of symmetric and antisymmetric structural modes, and n_{a_s} and n_{a_a} are the number of symmetric and antisymmetric aerodynamic states.

V. Asymmetric LCO in Response to Step Aileron Deflection

The ASE plant model of Eq. (6) was first constructed with the assembly of the FM symmetric modes of Table 1 and the respective antisymmetric modes. It was then implemented in Simulink with the nonlinear feedback moments of Eq. (11) based on the modal response and actuator outputs of Eq. (9), with the aircraft roll rate measured at the centerline point near the aircraft c.g. The next simulations are deviations from a steady level flight at $V = 25$-m/s sea level, with the free-play angle $\delta_f = 0.5$ deg and actual aileron angle $\delta_t = -1$ deg at both wings. The right- and left-aileron elastic deflections δ_{s_r} and δ_{s_l} are relative to the initial δ_t. A roll simulation was performed, starting with an antisymmetric step actuator command $\delta_c = 3.67$ deg that brings the right aileron to the free-play zone, using the initial conditions $\{x_{ae}(0)\} = \{0\}$. The resulting right- and left-aileron elastic deflections are given in Fig. 4. It can be

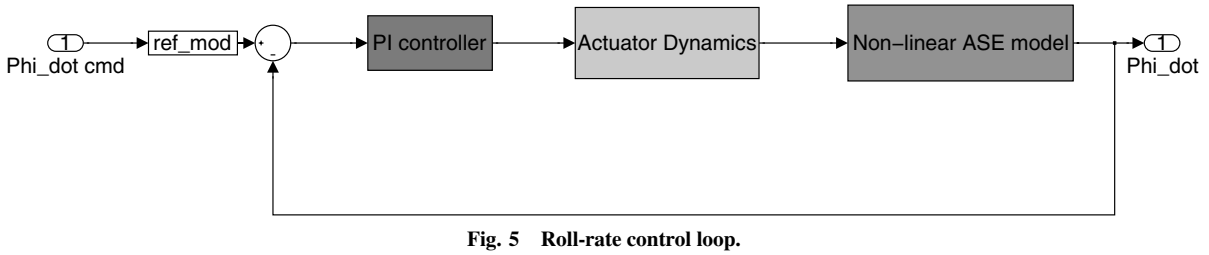

Fig. 5 Roll-rate control loop.

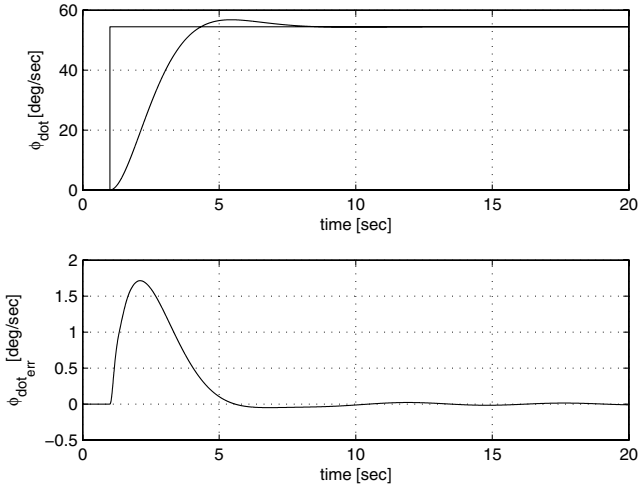

Fig. 6 Closed-loop response with no free play; $\dot{\phi}_{cmd} = 1.0$ rad/s.

observed that the right aileron experiences almost harmonic oscillations at 5 Hz, with amplitude slightly larger than the free-play zone. The left aileron also vibrates at the same frequency, but with much smaller amplitude. It should be emphasized that an asymmetric flutter is obtained even though the linear flutter mechanism is symmetric, due to structural feedback that couples the symmetric and the antisymmetric modes.

VI. LCO During Roll Maneuvers of a Controlled Vehicle

The analyses and simulations presented in this section are for lateral maneuvers initiated at the same steady conditions of the previous sections. The nonlinear roll simulations were performed using the full nonlinear ASE plant model of the previous section augmented with a third-order actuator and a classical proportional–integral (PI) controller designed to regulate the aircraft roll rate as measured at the centerline through commands to the aileron actuators.

The roll-rate control loop is shown in Fig. 5. The linear PI controller design is based on the linear ASE plant (without free play).

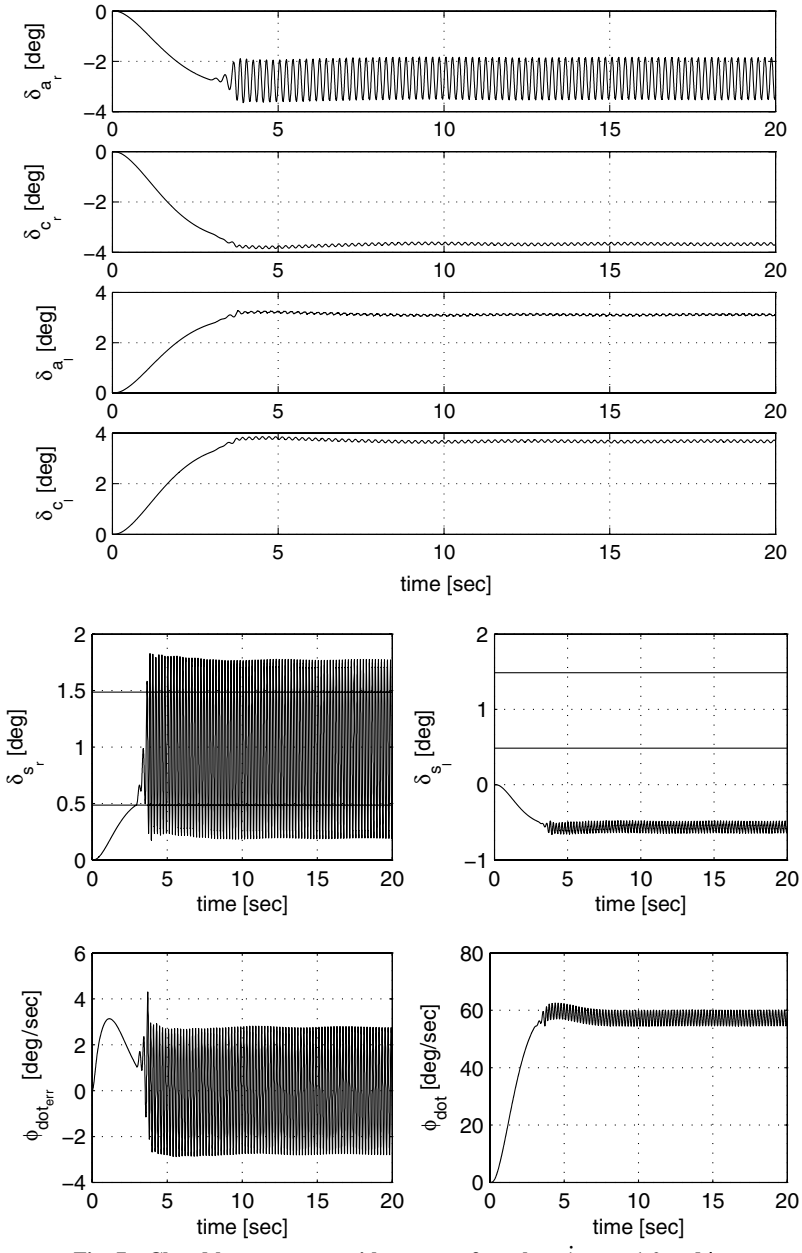

Fig. 7 Closed-loop response with actuator free play; $\dot{\phi}_{cmd} = 1.0$ rad/s.

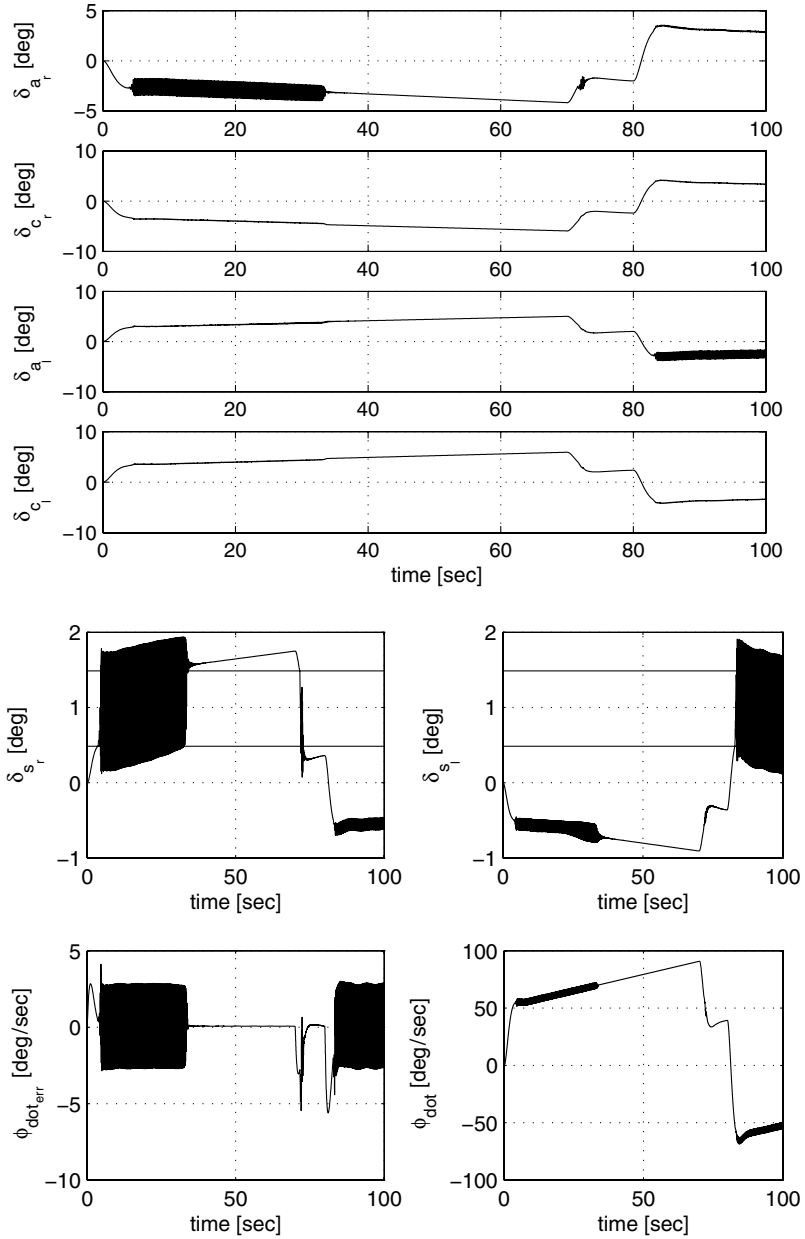

Fig. 8 Closed-loop response with actuator free play in a typical roll maneuver.

The input to the controlled system is the reference tracking-signal roll-rate command, generated by a reference model forced by an external input (e.g., pilot roll-rate command). The reference model is a second-order filter with a natural frequency $\omega = 5$ rad/s and damping coefficient $z = 0.7$. The roll-rate error signal is fed through the PI controller, which generates an aileron deflection command to third-order actuator dynamics for both right and left ailerons with opposite signs to achieve the desired roll maneuver. The PI controller was designed to guarantee acceptable closed-loop stability margins for the no-free-play case. Time histories of a characteristic system response for the no-free-play case to roll-rate step input command $\dot{\phi}_{\text{cmd}} = 1.0$ rad/s are shown in Fig. 6, demonstrating accurate tracking and adequate closed-loop behavior.

With the free-play zone, response parameters to the same roll-rate step input command are shown in Fig. 7. The appearance of LCO for the right aileron could be observed, with small effects on the left aileron. The maneuver is such that the right aileron is brought to the middle of its free-play zone and stays there. A system response to a more complex typical time-varying roll maneuver is shown in Fig. 8. It can be observed that each aileron experiences LCO while passing through its free-play zone and that the oscillation centers move in the direction of the commanded deflections. When the command rate is such that an aileron crosses its free-play zone quickly, as near $t = 70$ s, the vibrations do not have time to develop. The modal response in such simulations can be used to determine the stress load levels and accelerations in the structure while the vehicle experiences LCO, to define the associated dangers, design requirements, and control means to overcome LCO and/or its effects.

VII. Conclusions

An efficient methodology for the construction of modal-based, time-domain, state-space aeroservoelastic equations of motion with large local structural nonlinearities was presented. The use of fictitious masses when generating the modal data bases allows large variations of local stiffness properties without returning to the finite element model. Simulation models were constructed in which local nonlinearities were introduced via feedback loops while the plant remained linear. The method was applied in a highly accurate manner to the construction of controlled-maneuver ASE simulation models of a UAV, with the control-surface actuators exhibiting free play while changing the hinge moment sign. The simulation model was developed using a united set of symmetric and antisymmetric

low-frequency modes for obtaining asymmetric aircraft response due to stiffness asymmetry in the nonlinear elements. The direct-force approach to the application of control forces was shown to be more adequate in cases in which actuators became disconnected. Limit-cycle oscillations were developed in lateral maneuver simulations of the UAV. The oscillation started in the free-play zone as a regular control-surface flutter near the first symmetric wing-bending frequency and reached constant-amplitude oscillations after exceeding the free-play zone. The model facilitates the extraction of structural and control design parameters during the LCO, which can be used to assess the LCO effects on ride comfort and structural integrity. It was shown that when driven quickly across the free-play zone, the full oscillations may not have sufficient time to develop. The model construction and the simulation process rely on commercially available finite element, ASE, and simulation codes. The state-space models can be readily used for control augmentation using standard control design codes and for the design of LCO alleviation, which is beyond the scope of this paper.

Acknowledgment

The excellent advice and technical support provided by Moshe Idan of Technion—Israel Institute of Technology throughout the work that led to this paper are gratefully acknowledged.

References

[1] Karpel, M., "Design for Active Flutter Suppression and Gust Alleviation Using State-Space Aeroelastic Modeling," *Journal of Aircraft*, Vol. 19, No. 3, 1982, pp. 221–227.

[2] Karpel, M., "Time-Domain Aeroservoelastic Modeling Using Weighted Unsteady Aerodynamic Forces," *Journal of Guidance, Control, and Dynamics*, Vol. 13, No. 1, 1990, pp. 30–37.

[3] "ZAERO Version 7.0 Theoretical Manual," ZONA Technology, Scottsdale, AZ, Nov. 2003.

[4] Dowell, E. H., Tang, D., "Nonlinear Aeroelasticity and Unsteady Aerodynamics," *AIAA Journal*, Vol. 40, No. 9, 2002, pp. 1697–1707.

[5] Dowell, E. H., Edwards, J. W., and Strganac, T. W., "Nonlinear Aeroelasticity," *Journal of Aircraft*, Vol. 40, No. 5, Sept.–Oct. 2003.

[6] Croft, J., "Airbus Elevator Flutter: Annoying or Dangerous?," *Aviation Week and Space Technology*, Vol. 155, No. 9, Aug. 2001, p. 41.

[7] Conner, M. D., Virgin, L. N., and Dowell, E. D., "Accurate Numerical Integration of State-Space Models for Aeroelastic Systems with Free Play," *AIAA Journal*, Vol. 34, No. 10, 1996, pp. 2202–2205.

[8] Demourant, F., and Pavie, A., "Frequency Domain Analysis of the Aeroelastic Stability with a Control Surface Freeplay," *Proceedings of the International Forum on Aeroelasticity and Structural Dynamics* [CD-ROM], Royal Institute of Technology (KTH), Stockholm, Sweden, June 2007, Paper IF-014.

[9] Karpel, M., and Raveh, D., "Fictitious Mass Element in Structural Dynamics," *AIAA Journal*, Vol. 34, No. 3, 1996, pp. 607–613.

[10] Karpel, M., and Wieseman, C. D., "Time Simulation of Flutter with Large Stiffness Changes," *Journal of Aircraft*, Vol. 31, No. 2, 1994, pp. 404–410.

[11] Karpel, M., and Moulin, B., "Models for Aeroservoelastic Analysis with Smart Structures," *Journal of Aircraft*, Vol. 41, No. 2, Mar.–Apr. 2004, pp. 314–321.

[12] Livne, E., "Accurate Calculation of Control Augmented Structural Eigenvalue Sensitivities Using Reduced Order Models," *AIAA Journal*, Vol. 27, No. 7, 1989, pp. 947–954.